SAN02000-1773J

Adsorption of Barium(II) on Montmorillonite Surface

Peng-Chu Zhang*, Pat V. Brady and Sara E. Arthur

Geochemstry Department, MS 0750

Sandia National Laboratories

Albuquerque, NM 87185

Wei-Qing Zhou[†], Dale Sawyer[†], and Dean A. Hesterberg[=]

Departments of [†]Physics, [=]Soil Sciences

North Carolina State University

Raleigh, NC

*Corresponding author, MS 0750, Sandia National Laboratories, Albuquerque, NM 87185, USA. (505) 856-3677, pzhang@sandia.gov

DISCLAIMER

DISCLAIMER

Portions of this document may be illegible in electronic image products. Images are produced from the best available original document.

Abstract

Migration of radioactive radium, ^{226}Ra, in soil is an environmental concern, especially in areas adjacent to the uranium processing facilities. Barium(II), as Ba^{2+}, was used as a Ra analog and reacted with a Na-montmorillonite to obtain mechanistic insights into the interaction of Ra with soil matrices. The majority of sorbed Ba is associated with the permanently charged surface sites on the montmorillonite basal surface. This is indicated by: 1). sorption of Ba(II) on montmorillonite is not highly sensitive to solution pH, although a slight increase of sorption was observed at higher pH values; and 2) displacement of sorbed Ba increased with increased $NaNO_3$ concentration. As demonstrated by EXAFS, the Ba adsorbed on the montmorillonite edge, although it is a small fraction of the total sorbed Ba, forms an inner-sphere surface complex through sharing of oxygen atom(s) from deprotonated –OH group of the Al octahedral layer. The EXAFS measured distances between Ba and O at the first shell and Ba and Al of the second shell are 2.7 –2.8 and 3.7 – 3.9 Å, respectively, consistent with the results from geometry of a inner-sphere complex at the edge site. Results from bulk experiments and spectroscopic analysis suggest a co-existence of outer- and inner-sphere surface complexes at the Ba sorbed montmorillonite surface.

Key Words: Barium, Sorption, EXAFS, montmorillonite, Radium

Introduction

Radium, ^{226}Ra ($t_{1/2}$ = 1,600 years), is a decay product of uranium and thorium, either natural-occurring or discharged from uranium processing facilities [1-4]. The fate and behavior of ^{226}Ra in soil and sediment directly affects the dose of public exposure to radioactivity for the Ra decay daughter product, Rn, is responsible for 55% of this type of radioactivity [5]. Compared with U, Ra has a higher mobility in the soil profile and higher accessibility to food web. The activity ratio (AR) of $^{226}Ra/^{238}U$ in the soil is about 0.1, but ^{226}Ra greatly exceeds ^{238}U activity in most surface soil (AR up to 1.8) and in vegetation (AR up to 65) [6]. However, except for a limited bulk study [7], the mechanisms of the interaction between Ra and soil constituents such as clays, oxides and soil organic matters remain relatively unknown. To obtain a mechanistic understanding of Ra interaction with soil, Ba is employed here as a Ra analog and for reaction with montmorillonite, a common soil mineral. Barium is an ideal analog of Ra as Ba and Ra are the alkaline earth elements, and possessing similar ion radius (Ba^{2-} = 1.34 Å and Ra^{2-} = 1.43 Å) [8].

Adsorption of divalent alkaline earth ions, including Mg^{2-}, Ca^{2-}, Sr^{2-} and Ba^{2-}, on clay mineral and hydroxide surfaces has long be considered to occur by formation of an outer-sphere surface complex of the metal ion and the negatively charged surface at the solid/solution interface, though there is no differentiation among the surfaces (e.g., [9]). This is based on the well known Irving-Williams series that describes the relative ability to form coordinative complexes; the association of the alkaline earth ions with the surface

hydroxyl sites are attributed to electrostatic attraction. This theory successfully explains decreased adsorption of alkaline earth ions with increasing ionic radii [10]. Compared with adsorption of divalent transition cations, Cu^{2-}, Ni^{2-} and Co^{2-}, divalent alkaline earth ions are less susceptible to hydroxide complexation. However, when the soft Lewis base site, e.g., the basal layer of smectite, dominates the surface, adsorption will correlate with acid hardness and the Hoffmeister series will be followed: $Mg^{2-} < Ca^{2-} < Sr^{2-} < Ba^{2-}$ [9]. This order describes sorption at interlayer siloxane ditrigonal cavities on smectite [11].

Outer- and inner-sphere surface complexes are the two primary configurations of sorbed cations. 'Weak' outer-sphere complexes sorb on the surface with at least one water molecule between the surface site and the metal. The adsorbed metal ion is easily replaced by cations such as Na^{-} and K^{-} and therefore, is strongly affected by the ionic strength. When a metal ion is directly coordinated with the surface site, in most cases sharing an oxygen atom with the surface hydroxyl function group, an inner-sphere complex is formed. This kind of complex usually involves stronger bonding between the surface and sorbed metal and is not strongly affected by simple electrolyte cations such as K^{-} and Na^{-}.

Montmorillonite is present in most soils and aquatic systems. Substitution of Fe(II) and Mg(II) for Al(III) in the octahedral layer creates a positive charge deficit and gives a net permanent negative charge to the surface. In contrast, the O and OH atoms on the broken edges of the montmorillonite hydrolyze and form Lewis acid and base function groups from which pH-dependent charge originates.

In addition to conducting bulk sorption/desorption measurements, in this study, synchrotron based X-ray absorption fine structure spectroscopy (XAFS) was employed to investigate the molecular scale nature of the interaction of Ba(II) at the montmorillonite surface. This knowledge is needed to understand behavior of Ra(II) migration in subsurface environments, to plan remediation strategies for contaminated soils and groundwaters, and to develop effective clay barrier systems.

Materials and Procedures

Montmorillonite (SWy-1) was obtained from the Source Clay Repository of the Clay Mineral Society (University of Missouri, Columbia, MO). Properties such as surface area (31.82 $m^2 g^{-1}$) and cation exchange capacity (CEC, 76.4 cmole kg^{-1}) are documented in the Repository home page (http://missouri.edu/geoscjy/SC/). Prior to use, the clay was placed in 1.0 M $NaNO_3$ solution for four days and the solution was changed daily to displace other exchangeable cations on the clay surface with Na^+. The clay was then dialyzed in a water bath to remove excess $NaNO_3$. After dialysis, the clay suspension was allowed to settle in a 2-liter beaker for four days. The blackish particles that settled with the clay at the bottom were discarded. The solid concentration of the suspension was determined by drying a known volume of clay suspension at 105° C for 24 hours. The clay suspension was agitated on a shaker to assure that the suspension was homogenized when subsamples were taken for an adsorption experiment.

Adsorption Experiments

Adsorption of Ba(II) on montmorillonite was conducted under: 1) variable $NaNO_3$ concentrations but constant pH; and 2) variable pH but constant $NaNO_3$ concentration. In all experiments, the initial concentration of Ba(II), added as $Ba(NO_3)_2$, was 5.0 mmol L^{-1}, and the montmorillonite clay concentration was held constant at 10.0 g L^{-1}.

In constant $NaNO_3$ concentration experiments, pH was initially adjusted to 3.5, 4.0, 5.0, 6.0, 7.0, 8.0 and 9.0 with 0.1 N HNO_3 or NaOH solution. The $NaNO_3$ concentration was adjusted to 0.002 M with a 0.1 N $NaNO_3$ solution.

In the variable $NaNO_3$ concentration experiment, adsorption was measured at two pH levels: 6.2 – 6.5 and 7.2 – 7.4. Three $NaNO_3$ concentrations, 0.002, 0.08, and 0.15 M, were used.

It should be pointed out that Ba^{2-} was the predominant species of Ba(II) in the aqueous phase for all treatments. No Ba-bearing solids were saturated under the conditions of the experiment.

After ~12 hrs agitation, the Ba(II)-containing montmorillonite suspensions were centrifuged at 4,000 rpm for 30 minutes. The supernatants were then filtered through a 0.2 μm membrane. The filtrates were analyzed on a direct coupled plasma spectrophotometer (DCP) for Ba(II). The differences between the added and remaining

Ba(II) in the solution were attributed as the results of Ba(II) adsorption on montmorillonite.

XAFS Analysis

After centrifugation, a portion of suspension was preserved in an air-tightened plastic tube and kept as a paste-like wet phase in a refrigerator for XAFS analysis.

XAFS analysis was conducted at beamline X-11A National Synchrotron Light Source at Brookhaven National Laboratory (NSLS/BNL). Along with the clay samples, several Ba(II) solids as well as aqueous Ba(II) were examined. XAS data was acquired at the Ba L_{III}-edge of 5,274 eV. The electron beam energy was 2.5 GeV and the beam current was between 200 and 350 mA. The monochromator consisted of two parallel Si(111) crystals with an entrance slit of 0.5 mm. The spectra were collected at room temperature. A multi-element Ge solid state detector (11 working channels) was used for detection in fluorescence mode.

XAFS data analysis was accomplished using the program MacXAFS 4.0 with standard reduction practice, pre-edge subtraction, normalization, Fourier transform and, finally, nonlinear least square fitting. The multiple shell fitting were performed in r-space, where reference bond information (Ba-O, Ba-Al/Si, and Ba-C) were either generated by FEFF code or from the structural data for standard samples, such as crystalline $Ba(OH)_2$, $BaCO_3$ and aqueous $Ba(NO_3)_2$. These standard compounds are used to improve the

accuracy in data fitting and aqueous Ba^{2+} would serve an analogue for outer-sphere surface complexes.

RESULTS

Adsorption of Ba(II) on montmorillonite: Effect of pH and $NaNO_3$ Concentration

The pH-dependent Ba adsorption on montmorillonite is shown in Figure 1. At a $NaNO_3$ concentration of 0.002 M, Ba(II) adsorption increased with solution pH from 0.14 mmol g^{-1} at pH 4.3 to approximately 0.20 mmol g^{-1} at pH 8.5. Considering the CEC of montmorillonite, 76.4 meq 100 g^{-1}, adsorption of Ba(II) occupied 37 to 52% of the exchange sites of the clay in the pH range of 4.3 to 8.5. Adsorption of Ba(II) on montmorillonite is not as sensitive to pH compared to other mineral surfaces, such as on goethite (unpublished data). The pH-insensitive cation adsorption on montmorillonite or other smectite clay mineral surfaces has been observed elsewhere [12,13] and suggests that the majority of the adsorbed cation resides on the fixed negative charge site of the basal layer. Adsorption via fixed charge sites is pH independent and the adsorbed Ba(II) is thought to form outer-sphere complexes on the montmorillonite surface. However, for the hydroxyl surface site at the cleavage edge, adsorption should depend on pH because of the involvement of protonation/deprotonation processes. Therefore, increased Ba(II) adsorption with pH is attributed to surface complex formation on the hydroxyl sites at the clay edge. Although the adsorption isotherm is not pH sensitive, the amount of adsorbed Ba(II) due to increasing pH can't be ignored as demonstrated in Figure 1.

In contrast, the effect of $NaNO_3$ concentrations on Ba(II) adsorption is much more profound. In the two tested pH ranges, pH 6.2 – 6.5 and pH 7.2 – 7.4, adsorption of Ba(II) is depressed from 0.18 to 0.06 and from 0.16 to 0.01 mmol g^{-1}, respectively, as $[NaNO_3]$ increases from 0.002 to 0.15 mol L^{-1} (Figure 2). The difference of the amount of adsorbed Ba(II) ranges from threefold to more than one order of magnitude in the $NaNO_3$ concentration ranging from 0.002 to 0.15 mol L^{-1}. Compared with adsorption from the variable pH experiment shown in Figure 1, the difference in Ba(II) adsorption between low and high pH was only 30%. Adsorption of Co(II) and Pb(II) on montmorillonite was also reported as pH insensitive and sensitive to the ionic strength, or NaCl concentration [12-14].

These observations indicate that adsorbed Ba(II) is selectively displaced from the clay surface at low to neutral pH and high $[NaNO_3]$, but a portion of it remains sorbed at higher pH regardless of the $[NaNO_3]$. The strong adsorption of Ba(II) at high pH has also been documented elsewhere [8,14-16].

EXAFS Analysis

The normalized k^2-weighted EXAFS spectra of Ba(II) sorbed on montmorillonite under various pHs and $NaNO_3$ concentrations are shown in Figure 3. Spectra for crystalline $Ba(OH)_2$ and the aqueous $Ba(NO_3)_2$ solution are also included for comparison. The top three spectra from in Figure 3 were obtained from samples with the same pH but varying

$NaNO_3$ concentration. The rest are from constant $NaNO_3$ concentration and various pH. Correspondingly, Figure 4 illustrates phase-uncorrected radial structure functions (RSFs) generated from Fourier transforms over the k^2-weighted EXAFS spectra from 1.4 to 9.3 $Å^{-1}$. Since the Fourier transforms are phase-uncorrected, the peak positions in Figure 4 are generally shorter by roughly 0.4 Å compared to the corresponding bound distances. Peaks with R = 2.4 Å represent the Ba-O bond distance with the real distance of approximately 2.7 –2.8 Å. The peaks with R = 3.3 - 3.4 Å are only observed in the Ba-montmorillonite samples and are attributed to the higher-shell coordination of adsorbed Ba(II) with Al or Si in the octahedral or tetrahedral layers of montmorillonite, respectively. There is no definitive structure determined beyond the first shell of hydrated oxygen atoms for the aqueous Ba(II) (Figure 4). However, crystalline $Ba(OH)_2$ has a predominant peak at about 4.1 Å as shown in Figure 4, which corresponds a Ba-Ba bond distance at 4.42 Å. Comparison of the reference and Ba adsorbed samples give us clear indication of surface structures.

Figure 5 shows that the EXAFS spectra for Ba(II) adsorbed on the montmorillonite surface are best described by a fit that includes Si/Al as the second-neighbor backscattering atom. This figure shows the k^2-weighted filtered experimental EXAFS spectra (solid line) in comparison with theoretic spectra (dashed line) of the second RSF peak of a Ba-montmorillonite sample presented in Figure 4 in which pH = 8.0 and $[NaNO_3]$ = 0.002 mol/L. When Si/Al are considered as second-neighbor backscattering atoms, a good agreement with the Fourier back-transformed XAFS spectrum is observed (Figure 5a). The contributions of the possible atoms in the system, O and Al/Si for the

first and second shells, to the best fit are shown in Figure 5b, respectively. In the fitting processes, other elements such as Ba were used as the second neighbor backscattering atoms and a poor quality of fitting resulted.

The non-linear, least squares fitting results of EXAFS analysis, including coordination number (CN), bond distances, and Debye-Waller factors ($\Delta\sigma^2$), are presented in Table 1.

The first peaks as shown in Figure 4 are all identified as the Ba-O bond. The oxygen coordination numbers in all adsorbed samples are in the range of 6 to 7 with an error bar of ±20%, which indicate that the Ba(II) associating with surrounding oxygen has an octahedral coordination or possibly, the sorbed Ba(II) is in a higher coordination with the ditrigonal cavity at the montmorillonite basal layer, fitting into the ditrigonal cavity like K^+ (radius = 1.33 Å). The Ba-O bond distances are in the range of 2.76 – 2.80 Å, similar to those either in the solid crystalline $Ba(OH)_2$, 2.78 Å, or in aqueous Ba(II), 2.79 Å. Note that at the same pH value the Ba-O bond distances decreased from 2.80 Å at lower $NaNO_3$ concentration, 0.002 M, to 2.73 Å at higher concentration of 0.15 M. This reduction in the distance may indicate an increase in bond strength for Ba(II) adsorbed on the hydroxyl sites at high ionic strength.

For the second shell in the Ba(II) coordination environment, best fits were obtained by identifying Si or Al as the second-neighboring atoms. Because Si and Al only differ in atomic number by 1, their backscattering amplitudes and phase structures are very similar. It is not practical to differentiate between them from the EXAFS spectra. The Ba-

Si/Al coordination numbers are all at about 2.0±0.4. The radial distances of Ba-Si/Al bond distance are about the same at 3.88±0.03 Å for the samples at various pH values but at the same $NaNO_3$ concentration of 0.002 M. However, the radial distance of Ba-Si/Al in the samples with different $NaNO_3$ concentrations decreases from 3.89 to 3.73 Å when $NaNO_3$ concentration increases from 0.002 to 0.15 M (Table 1). This could be attributed to the various configurations of Ba(II) at the hydroxyl surface sites and is discussed below. In all of the spectra from Ba(II) adsorption samples in this study, a Ba-Ba distance at 4.42 Å, as in the $Ba(OH)_2$ crystal, is absent, indicating an absence of polynuclear Ba complexes at the surface. There was one noticeable difference among the samples studied at lower pH (4.3). There are additional Ba-O peaks at 3.20±0.03 and 3.56±0.03 Å with coordination number of 1.2 and 1.5, as shown in Figure 4 (uncorrected phases). There is no satisfactory explanation for these peaks. We suggest that this is related to a more defined structure of Ba(II) and oxygen at lower pH than at high pH.

DISCUSSION

Adsorption of Ba^{2-}, along with other divalent alkaline earth metal ions such as Mg^{2-}, Ca^{2-} and Sr^{2-}, on clay surfaces has long been considered to be non-specific, i.e., involving outer-sphere surface complexes [9]. This prediction is based on the use of hydrolysis constants of metal ions. The first hydrolysis constants of alkaline earth metals are lower than that of divalent transtion metal cations such as Co^{2-}, Ni^{2-} and Zn^{2-} [9], which form inner-sphere complexes at the clay surface. Other evidence supporting this hypothesis includes the slight effect of ionic strength on adsorption. Generally, alkaline

earth metal sorption is depressed when solution electrolyte concentration increases [17-20]. The divalent alkaline earth cations adsorbed on surfaces are "exchangeable", since there are no strong chemical bonds formed between the surface functional groups and the sorbed ions. Most of these observations are from macroscopic studies. Recent evidence from EXAFS study [12] seems to support this conclusion that there was no Al or Si found in the second shell of Sr(II) sorbed on montmorillonite surface. However, there are exceptions. It has been recognized for years that sorbed Pb^{2+} forms inner-sphere surface complexes on a number of oxide surfaces and clay surfaces, as indicated by bulk studies or spectroscopic studies [21-32]. But, recent XAFS studies indicate that sorbed lead ion, Pb^{2+}, can form outer-sphere complexes on Al oxide [14] and clay surfaces [33] at low ionic strength and near neutral pH yet adsorption is strongly affected by solution ionic strength. Coexistence of outer- and inner-surface complexes, therefore, was suggested.

As shown in Figure 1 even at a low pH of 4.3, significant Ba(II) adsorption was observed. Since cation adsorption on the fixed charge sites is insensitive to solution pH, adsorption at low pH can be attributed to uptake by the negative charged sites located at the basal layer. This type of adsorbed cation is considered to be an outer-sphere complex or "exchangeable", because the driving force of adsorption is electrostatic attraction. There is no formation of relatively strong chemical bonds, but rather a weak association between the cation and surface. Adsorbed cations, in this case, Ba^{2+}, can be displaced by cations (Na^+) present in greater quantity. This results in a decrease in Ba(II) adsorption when $NaNO_3$ concentration increases (Figure 2).

Increased adsorption of Ba(II) at high pH (Figure 1 and 2) occurs due to deprotonation of the hydroxyl group at the mineral edge. It is also noticed that when $NaNO_3$ concentration reached 0.15 M, a small portion of Ba(II) is still associated with the surface. These observations suggest formation of a stronger surface complex at the hydroxyl sites. From the EXAFS data, it is reasonable to propose that formation of inner-sphere complexes occurs, in addition to outer-sphere complexes. Although we were not able to locate a mineral that contains Al/Si-O-Ba to serve as a reference in XAFS to estimate the bond distance and configuration of adsorbed Ba and Si or Al of the clay, the distance between adsorbed Ba(II) and Al/Si can be estimated from the literature. Adsorbed Ni(II) forms an inner-sphere complex on montmorillonite, the distance of adsorbed Ni atom and Si/Al is about 3.07 Å [34,35]. If we assume the same configuration of the Ni(II) with montmorillonite occurs in inner-sphere Ba(II) sorption, the distance between the adsorbed Ba(II) and Al/Si should be about 3.72 Å, which agrees well with EXAFS data (Table 1). The difference between Ni-Si/Al and Ba-Si/Al, 0.65 Å, is readily attributed to the difference between the radii of Ni^{2-} ion, 0.69 Å, and Ba^{2-} ion which is 1.34 Å. The distance between Co-Al, when Co(II) formed inner-sphere complex on the montmorillonite surface, is 3.15 Å [12]. Considering a 0.62 Å difference between Co(II) and Ba(II) radii, in the inner-sphere complex, the Ba(II)-Al distance should be in the range of 3.77 Å, which is also consistent with the results of this study (Table 1).

The distance between Ba(II) adsorbed on the deprotonated sites at the montmorillonite edge was geometrically examined using a graphical display of the montmorillonite crystal structure (WebViewer, MSI). This was done by placing a hydrated Ba^{2-} at the

edge of a montmorillonite structure. In this arrangement, the sorbed Ba(II), in an octahedral coordination, was allowed to share one oxygen atom with the Al octahedron at the montmorillonite interrupted edge. The Ba-O distance is about 2.76 – 2.85 Å, agreeing with that from EXAFS analysis (Table 1). The distance between Al and Ba(II), as determined from this configuration geometry, fell in the range of 3.71 – 3.8 Å as obtained from EXAFS (Table 1). A similar geometric analysis was performed for Ba-Si, assuming Ba(II) shares an oxygen with tetrahedral Si-O at the edge. The distances of Ba-O and Ba-Si, as calculated, can't be constrained in the range resulted from EXAFS analysis (Table 1). Therefore, adsorption Ba(II) on the Si tetrahedron at the clay edge was excluded. Considering the distance of Ba-Al obtained from EXAFS is a weighted average for all possible forms of connection between Ba and Al, e.g., edge to edge, corner to corner and face to face, the distances from EXAFS analysis and the geometry analysis agree reasonably well with each other. The measured distance between Al and Ba(II) is longer in the sample with low [$NaNO_3$] than that when the concentration is high, 3.89 vs. 3.73 Å for 0.002 and 0.15 $NaNO_3$ M, respectively (Table 1). We attribute this to a potentially different configuration of Ba(II) associated with the surface oxygen atoms. It is possible that Ba(II) associates with Al through sharing only one oxygen atom to form a monodentate, or corner to corner associate, instead of bidentate, or edge to edge association. The distance of monodentate Ba-Al should be longer than 3.73 Å. EXAFS analysis provides an average distance for the possible association between Ba and Al and therefore, it is reasonable to expect the portion of edge to edge connection in the high [$NaNO_3$] is higher than that in the low [$NaNO_3$] samples.

Theoretically, the differences between the two coordination configurations can be distinguished from the EXAFS spectra that represent the samples with predominant adsorption on the basal layer as the outer-sphere complex or at the clay edge formed as an inner-sphere complex. The EXAFS data indicates that formation of inner-sphere complexes occurred in all conditions of this study. The inner-sphere complex observed at pH = 4.3 and $NaNO_3$ = 0.002 M samples, may only represent a small portion of the adsorbed Ba(II), but its contribution to the spectrum is strong enough to be recognized and significant enough not to be ignored during data reduction and fitting. In another words, the backscattering in adsorbed Ba(II) second shell by Al are strong and distinguishable, and appear in each of the spectra regardless of the dominant configuration. EXAFS analysis in this study indicates the existence of inner-surface complexes of Ba(II) on montmorillonite, but not the absolute abundance. The latter can only be achieved by varying pH and in an ion exchange experiment such as shown in Figure 1 and 2.

The data presented here indicate that Ba(II) can form both inner- and outer-sphere complexes on the montmorillonite surface, instead of just the outer-sphere complex formation as previous studies have suggested. Recently, inner-sphere complex formation has been shown as one of the common mechanisms of metal adsorption on montmorillonite surfaces, especially at high pH and ionic strength [36-41], in addition to the predominant outer-sphere complex. Outer-sphere surface complexes containing transition metals form predominantly at the fixed charge sites (permanent charge sites) at the interlayer and inner-sphere complexes form at the variable charge sites, hydroxyl

surface sites, located at the edges of the smectite. Although the number of reports found for alkaline earth ion formation of inner-sphere complex on clay and oxide surfaces are limited, evidences can be found either directly or indirectly to support this hypothesis. Cs^+ has an ionic radius of 1.67 Å (Ba^{++} = 1.34 Å), is not polarized. Kim et al. [40] used evidence from NMR measurements to show that adsorption of Cs ion on illite involved both inner-sphere adsorption on the edges of the clay and outer-sphere adsorption on the basal plane of the clay. Strontium ion, Sr^{2+}, adsorption on clay surfaces has been classified as outer-sphere complex formation from the bulk or spectroscopic studies [12]. However, when Sr^{2+} is adsorbed on kaolinite surface, EXAFS indicates that 6.4 Al elements are included in the second shell of the Sr^{2+} with a Sr-Al distance of 3.41 Å [42]. This suggests formation of inner-sphere complex of adsorbed Sr ion on the Al octahedral layer of kaolinite. In addition, EXAFS measurements of adsorption of Sr^{2+} on a hydrous ferric oxide [43] shows Fe elements in the second coordination shell of the adsorbed Sr^{2+}, suggesting that Sr^{2+} forms an inner-sphere complex through sharing an oxygen with the structural Fe of the hydrous ferric oxide.

Acknowledgement

The authors wish to thank the U.S. Nuclear Regulatory Commission for supporting this research, Dr. J. Krumhansl (SNL) for technical discussion and assistance in analytical laboratory and Drs. J.J. Liang and R. Cygan (SNL) for their assistance in bond distance measurements.

Sandia is a multiprogram laboratory operated by Sandia Corporation, a Lockheed Martin Company, for the United States Department of Energy under contract DE-AC04-94AL85000.

References

[1] R. S. Wang, A. S. Y. Chau, F. Liu, H. Cheng, P. Nar, X. M. Chen,Q. Y. Wu, Journal of Radioanalytical and Nuclear Chemistry-Articles 171 (1993) 347.

[2] A. S. Paschoa, Applied Radiation and Isotopes 49 (1998) 189.

[3] D. E. Hutchinson,L. F. Toussaint, Applied Radiation and Isotopes 49 (1998) 265.

[4] M. Z. Min, J. P. Zhai,C. Q. Fang, Chemical Geology 144 (1998) 313.

[5] NCRP "Ionizing radiation exposure of the population of the United States," National Concil on Radiation Protection, 1987.

[6] D. J. Greeman, A. W. Rose, J. W. Washington, R. R. Dobos,E. J. Ciolkosz, Applied Geochemistry 14 (1999) 365.

[7] J. S. Nathwani,C. R. Philips, Chemosphere 5 (1979) 285.

[8] T. Shahwan, S. Suzer,H. N. Erten, Applied Radiation and Isotopes 49 (1998) 915.

[9] K. F. Hayes,L. E. Katz, in: P. V. Brady (Ed), Physics and Chemisty of Mineral Surfaces, CRC Press, 1996.

[10] C. P. Huang,W. Stumm, J. Colloid Interface Sci. 43 (1973) 409.

[11] G. Sposito The surface chemistry of soils; Oxiford University Press: New York, 1984.

[12] C. C. Chen,K. F. Hayes, Geochimica Et Cosmochimica Acta 63 (1999) 3205.

[13] C. Papelis,K. F. Hayes, Coll. Surfaces 107 (1996) 89.

[14] D. G. Strawn, A. M. Scheidegger,D. L. Sparks, Environ. Sci. & Technol. 32 (1998) 2596.

[15] A. M. Scheidegger, G. M. Lamble,D. L. Sparks, J. of Colloid and Interface Sci. 186 (1997) 118.

[16] S. P. Mishra,D. Tiwary, Applied Radiation and Isotopes 51 (1999) 359.

[17] J. M. Zachara, S. C. Smith, J. P. McKinley,C. T. Resch, Soil. Soc. Amer. J. 57 (1993) 1491.

[18] A. Grutter, H. R. Von Gunten, E. Rossler,R. Keil, Radiochim. Acta 65 (1994) 181.

[19] P. W. Schindler,W. Stumm, Eds. The surface chemistry of oxides, hydroxides and oxide minerals; J. Wiley & Sons: New York, 1987.

[20] J. A. Davis,D. B. Kent, in: M. F. Hochella, A. F. White (Ed), Mineral-Interface Geochem. (1990) 177.

[21] M. N. Benjamin,J. O. Leckie, J. Colloid Interf. Sci. 79 (1981) 209.

[22] K. Bunzl, W. Schmidt,B. Sansoni, J. Soil Sci. 27 (1976) 32.

[23] E. A. Forbes, A. M. Posner,J. P. Quirk, J. Soil Sci. 27 (1976) 154.

[24] B. R. Coughlin,A. T. Stone, Environ. Sci. Technol. 29 (1995) 2445.

[25] J. R. Bargar, S. N. Towle, G. E. Brown,G. A. Parks, J. of Colloid and Interface Sci. 185 (1997) 473.

[26] J. R. Bargar, G. E. Brown,G. A. Parks, Geochimica Et Cosmochimica Acta 62 (1998) 193.

[27] M. L. Farquhar, D. J. Vaughan, C. R. Hughes, J. M. Charnock,K. E. R. England, Geochimica Et Cosmochimica Acta 61 (1997) 3051.

[28] Z. S. Kooner, C. D. Cox,J. L. Smoot, Environ. Toxicol. and Chem. 14 (1995) 2077.

[29] D. P. Rodda, B. B. Johnson,J. D. Wells, J. of Colloid and Interface Sci. 184 (1996) 365.

[30] A. L. Roe, K. F. Hayes, C. Chisholmbrause, G. E. Brown, G. A. Parks, K. O. Hodgson,J. O. Leckie, Langmuir 7 (1991) 367.

[31] V. M. Tsukanova,K. P. Tikhomolova, Colloid J. 57 (1995) 833.

[32] J. R. Bargar, G. E. Brown,G. A. Parks, Geochimica Et Cosmochimica Acta 61 (1997) 2639.

[33] H. J. Ulrich,C. Degueldre, Radiochimica Acta 62 (1993) 81.

[34] A. M. Scheidegger, G. M. Lamble,D. L. Sparks, Environ. Sci. Technol. 30 (1996) 548.

[35] A. M. Scheidegger, D. G. Strawn, G. M. Lamble,D. L. Sparks, Geochim. Cosmochim. Acta. In Review (1997).

[36] G. N. White,L. W. Zelazny, Clays and Clay Minerals 36 (1988) 141.

[37] J. M. Zachara,J. P. McKinley, Aquatic Sciences 55 (1993) 250.

[38] J. M. Zachara,S. C. Smith, Soil. Soc. Amer. J. 58 (1994) 762.

[39] J. P. McKinley, J. M. Zachara, S. C. Smith,G. D. Turner, Clays & Clay Minerals 43 (1995) 586.

[40] Y. Kim, R. T. Cygan,R. J. Kirkpatrick, Geochim. Cosmochim. Acta 60 (1996) 1041.

[41] C. Papelis,K. F. Hayes, Colloids and Surfaces a-Physicochem. Eng. Aspects 107 (1996) 89.

[42] R. H. Parkman, J. M. Charnock, F. R. Livens,D. J. Vaughan, Geochimica Et Cosmochimica Acta 62 (1998) 1481.

[43] L. Axe, G. B. Bunker, P. R. Anderson,T. A. Tyson, Journal of Colloid and Interface Science 199 (1998) 44.

Table 1. Structural Information Derived from XAFS Data Collected Under Various Conditions.

Exp. Conditions		First Shell Ba-O			Second Shell Ba-Al		
pH	$NaNO_3$ (M)	CN ±20%	R(Å) ±0.02	$\Delta\sigma^2$ Å^2	CN* ±20%	R(Å) ±0.02	$\Delta\sigma^2$ Å^2
4.3	0.002	6.8	2.80	0.013	1.8	3.87	0.004
6.6	0.002	6.9	2.76	0.014	2.0	3.86	0.004
7.2	0.002	6.9	2.80	0.013	2.2	3.89	0.012
8.0	0.002	7.0	2.80	0.013	2.5	3.88	0.004
7.2	0.002	6.9	2.80	0.013	2.2	3.89	0.012
7.4	0.08	7.8	2.79	0.013	2.1	3.76	0.004
7.2	0.15	7.2	2.73	0.0021	2.5	3.73	0.004
$Ba(NO_3)_2$ (aqueous)		6.4	2.79	0.01			
					Ba-Ba		
$Ba(OH)_2$ (crystal)		6.0	2.78	0.0013	8.5	4.42	0.03

*the second shell coordination number is not sensitive in the data fitting.

Figure Captions

Figure 1. Adsorption of Ba(II) on montmorillonite as a function of pH.

Figure 2. Effect of $NaNO_3$ concentration of Ba(II) adsorption on montmorillonite at constant pH values.

Figure 3. k^2 weighted normalized x-functions for Ba-montmorillonite suspensions with various pH and $NaNO_3$ concentrations and the reference samples.

Figure 4. Fourier transforms (RSF) of the x-functions in Figure 3. Phase shift s not corrected. A Ba-Al/Si bond is found in all Ba-montmorillonite spectra. Ba-Ba bond is only found in $Ba(OH)_2$ solid.

Figure 5. Example of EXAFS data fitting for spectra collected from a Ba-montmorillonite suspension. Spectrum used here is obtained at pH = 8.0 and $[NaNO_3]$ = 0.002 M. a) the solid lines are for the original RSF and imaginary, the circles are the fitting results for RSF and imaginary, respectively, when Al is included in the fitting; b) these are the fitting results for two separate neighborhood shells of adsorbed Ba(II). the solid lines are for the first shell of Ba-O and the circles for the second shell of Ba-Al.

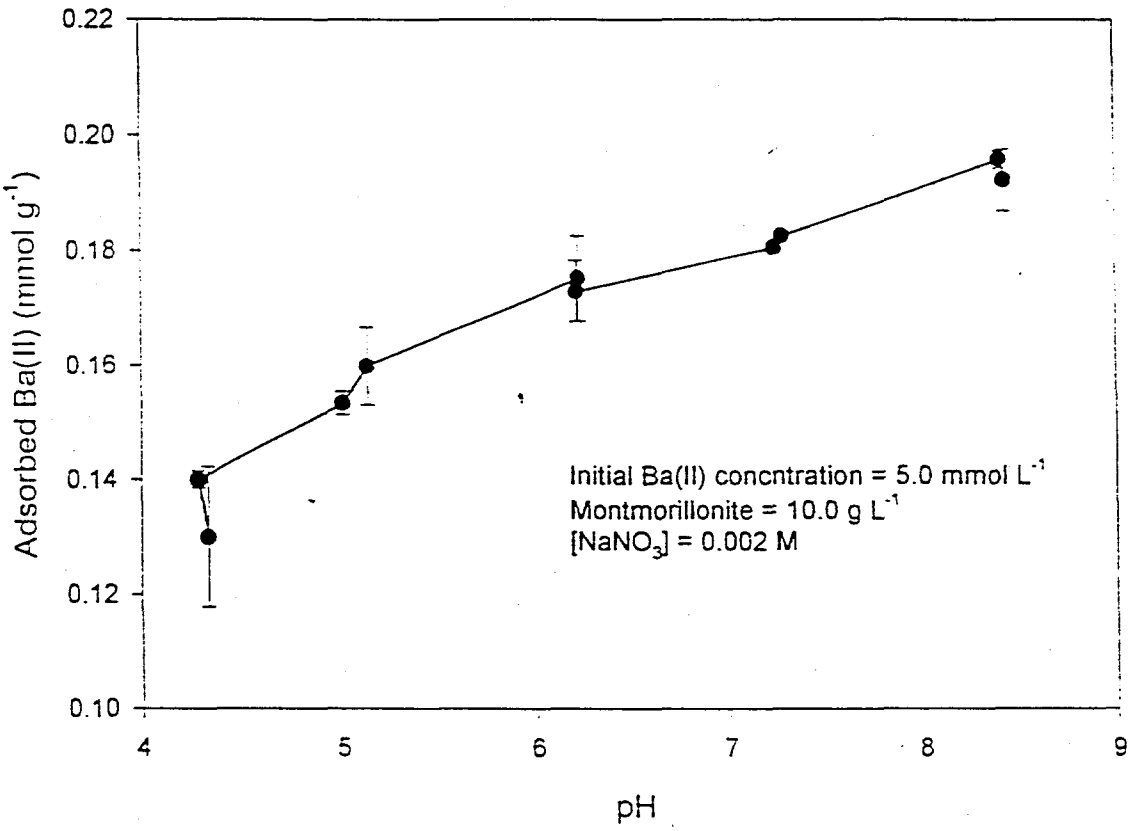
0.22
0.20
0.18
0.16
0.14
0.12
0.10
Adsorbed Ba(II) (mmol g-1)
4
5
6
7
8
9
pH
Initial Ba(II) concntration = 5.0 mmol L-1
Montmorillonite = 10.0 g L-1
[NaNO3] = 0.002 M

Fig 1

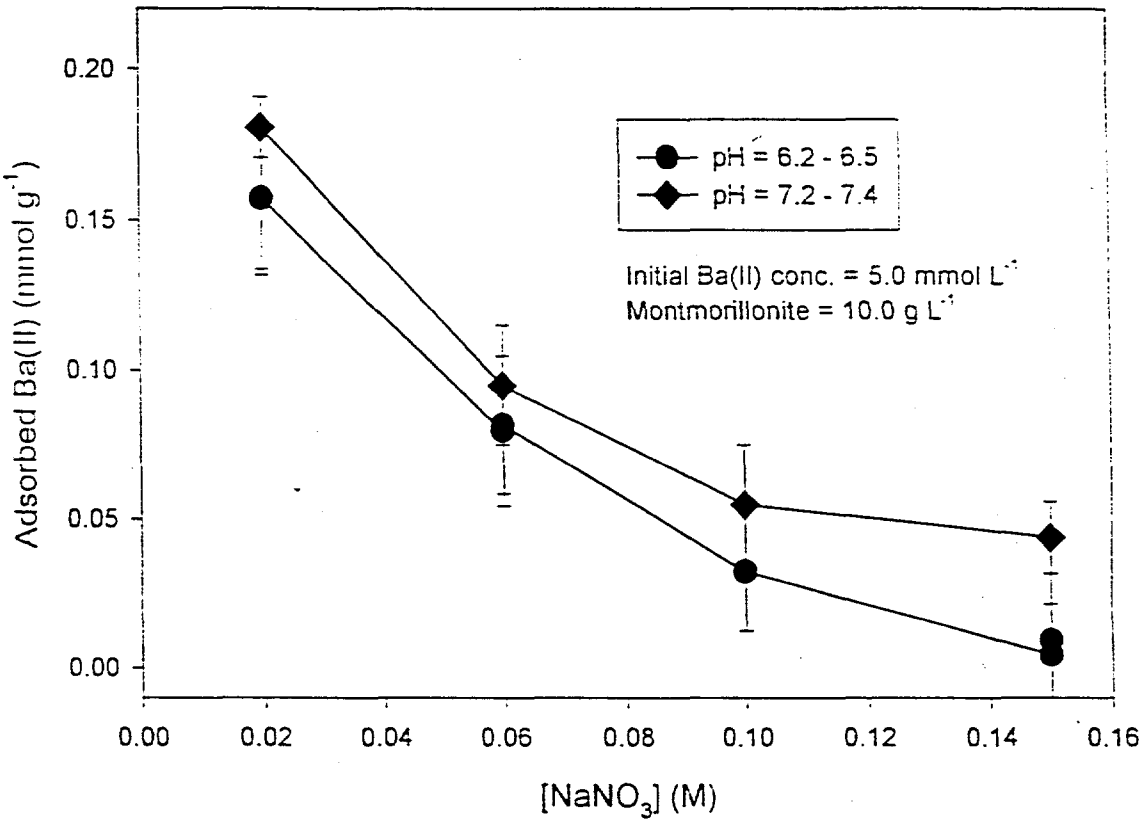
0.20
0.15
0.10
0.05
0.00
Adsorbed Ba(II) (mmol g-1)
pH = 6.2 - 6.5
pH = 7.2 - 7.4
Initial Ba(II) conc. = 5.0 mmol L-1
Montmorillonite = 10.0 g L-1
0.00
0.02
0.04
0.06
0.08
0.10
0.12
0.14
0.16
[NaNO3] (M)

Fig. 2

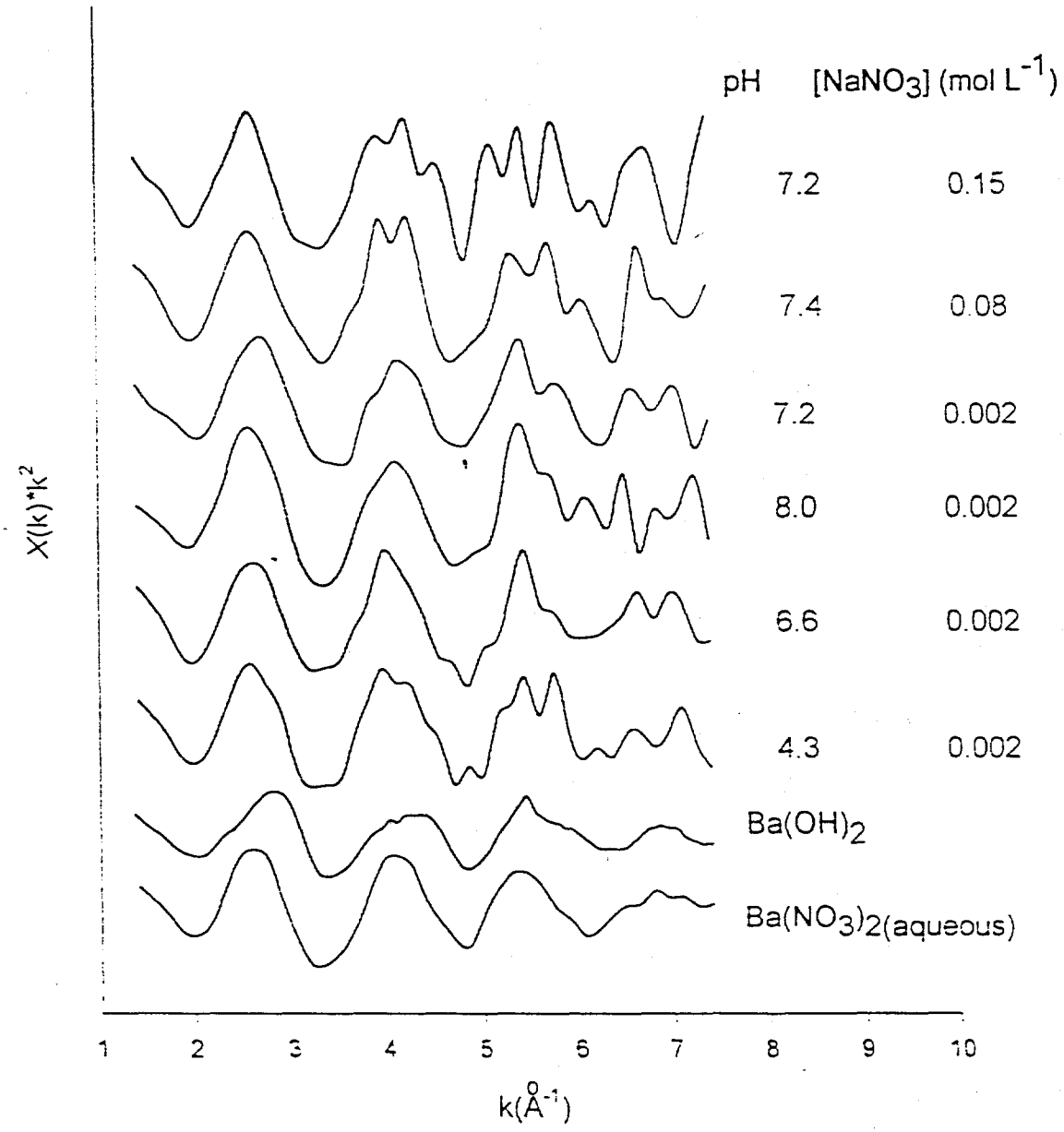
pH
[NaNO3] (mol L-1)
7.2
0.15
7.4
0.08
7.2
0.002
8.0
0.002
6.6
0.002
4.3
0.002
Ba(OH)2
Ba(NO3)2(aqueous)
X(k)*k2
1
2
3
4
5
6
7
8
9
10
k(Å-1)

Fig 3

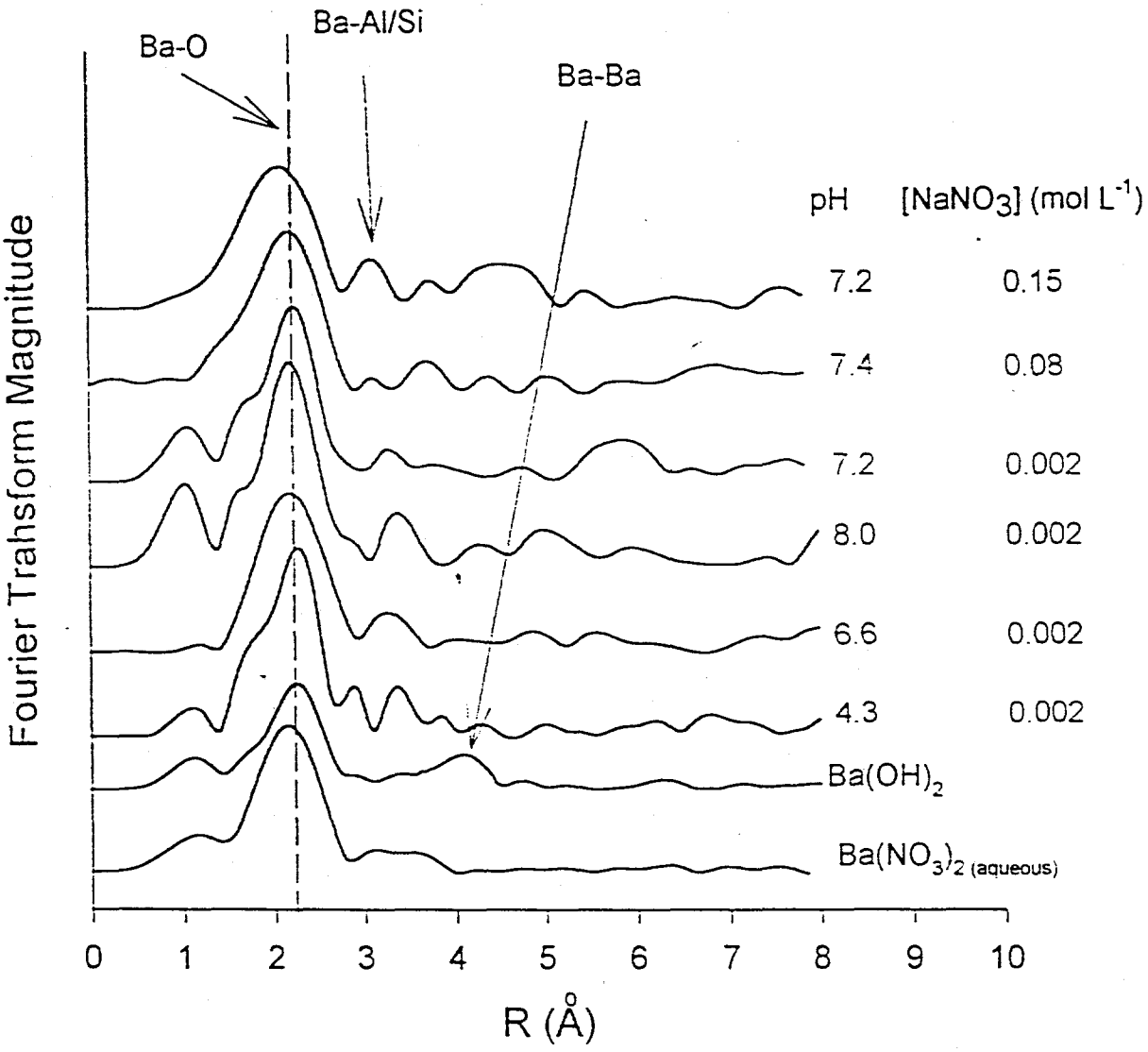
Ba-O
Ba-Al/Si
Ba-Ba
pH
[NaNO3] (mol L-1)
7.2
0.15
7.4
0.08
7.2
0.002
8.0
0.002
6.6
0.002
4.3
0.002
Ba(OH)2
Ba(NO3)2 (aqueous)
Fourier Trahsform Magnitude
0
1
2
3
4
5
6
7
8
9
10
R (Å)

Fig. 4

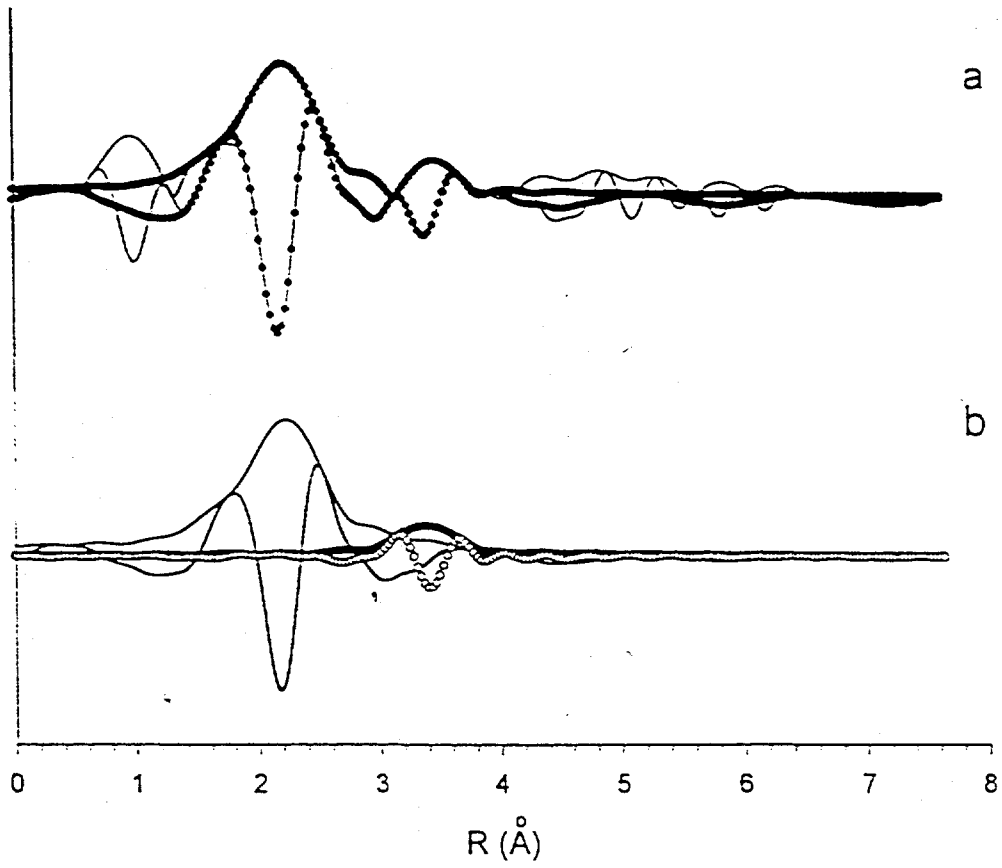

Fig. 5

Figure Captions

Figure 1. Adsorption of Ba(II) on montmorillonite as a function of pH.

Figure 2. Effect of $NaNO_3$ concentration of Ba(II) adsorption on montmorillonite at constant pH values.

Figure 3. k^2 weighted normalized x-functions for Ba-montmorillonite suspensions with various pH and $NaNO_3$ concentrations and the reference samples.

Figure 4. Fourier transforms (RSF) of the x-functions in Figure 3. Phase shift s not corrected. A Ba-Al/Si bond is found in all Ba-montmorillonite spectra. Ba-Ba bond is only found in $Ba(OH)_2$ solid.

Figure 5. Example of EXAFS data fitting for spectra collected from a Ba-montmorillonite suspension. Spectrum used here is obtained at pH = 8.0 and [$NaNO_3$] = 0.002 M. a) the solid lines are for the original RSF and imaginary, the circles are the fitting results for RSF and imaginary, respectively, when Al is included in the fitting; b) these are the fitting results for two separate neighborhood shells of adsorbed Ba(II). the solid lines are for the first shell of Ba-O and the circles for the second shell of Ba-Al.